RSC Advances

PAPER

View Article Online
View Journal | View Issue

Cite this: *RSC Adv.*, 2018, **8**, 25794

Insight into the capacity fading of layered lithium-rich oxides and its suppression *via* a film-forming electrolyte additive†

Jianhui Li, Lidan Xing,* Zaisheng Wang, Wenqiang Tu, Xuerui Yang, Yilong Lin, Yuqing Liao, Mengqing Xu and Weishan Li*

Received 5th May 2018
Accepted 3rd July 2018

DOI: 10.1039/c8ra03852j

rsc.li/rsc-advances

The capacity fading of layered lithium-rich oxide ($Li_{1.2}Mn_{0.54}Ni_{0.13}Co_{0.13}O_2$, LLO) cathodes greatly hinders their practical application in next generation lithium ion batteries. It has been demonstrated in this work that the slow capacity fading of a LLO/Li cell within 120 cycles is mainly caused by electrolyte oxidation and LLO phase transformation with Ni dissolution. After 120 cycles, the dissolution of Mn becomes worse than that of Ni, leading to structural destruction of the generated spinel phase structure of LLO and fast capacity fading. Tripropyl borate (TPB) is proposed as a film-forming electrolyte additive, which shows a great capability to enhance the cycling stability of LLO/Li, with a capacity retention improvement from 21% to 78% after 250 cycles at 0.5C. Electrochemical and physical characterization demonstrated that the TPB-derived SEI film shows great capability to suppress electrolyte oxidation and the structural destruction of the generated spinel phase of LLO.

1. Introduction

Lithium ion batteries (LIBs) have been applied as the most promising energy storage/conversion system because of their high operating voltage, high energy density and cost-effectiveness.[1–4] Although LIBs have been successfully commercialized, the energy density of LIBs needs to be improved to satisfy the demand of large-scale devices, such as electric vehicles (EVs) and hybrid electric vehicles (HEVs).[5–10] The energy density of conventional LIBs, with the cathodes, such as $LiCoO_2$ (~140 mA h g^{-1}) and $LiFePO_4$ (~160 mA h g^{-1}), operating at 3.3–3.9 V, is limited.[11,12] To achieve higher energy density, layered lithium-rich oxide (LLO) cathodes with chemical compositions of $xLi_2MnO_3 \cdot (1-x)LiMO_2$ (M = Co, Ni or Mn, $0 < x < 1$) are held in high esteem because of their high operating voltage (4.8 V) and high reversible specific capacity (200 mA h g^{-1}).[13] However, the application of LLOs has been greatly restricted due to their poor cycling stability, caused by the irreversible layered-to-spinel phase transformation upon cycling.[14–16] Moreover, carbonate-based electrolytes start to undergo oxidation at potentials beyond 4.3 V, generating polymers, gaseous products and HF. The former decomposition products increase the interfacial resistance and battery internal pressure, while the latter accelerates the structural transformation of the LLO.[17–22]

Great efforts to improve the structural and cycling stability of LLOs have been made, including surface coating (such as with Al_2O_3, ZrO_2, AlF_3, CaF_2 and polyaniline),[23–27] Na, K, La and Mg element doping[28–31] and the application of film-forming electrolyte additives.[32–36] The usage of a film-forming electrolyte additive, in comparison with the other methods, has the advantages of simple operation, high performance, and cost-effectiveness,[37] and the additive works by decomposing before the carbonate-based electrolyte to generate a solid electrolyte interface (SEI) film on the high voltage electrode surface. This SEI film effectively passivates the highly charged electrode surface, and therefore suppresses the direct electronic contact of the carbonate-based electrolyte with the electrode. The investigated film-forming electrolyte additives mainly include nitriles (such as 1,3,6-hexanetricarbonitrile and glycol bis(propionitrile) ether),[38,39] phosphites (such as trimethyl phosphite, triethyl phosphite, triphenyl phosphite and tris(2,2,2-trifluoroethyl) phosphite)[40–43] and silicohydrides (such as (trimethylsilyl)methanesulfonate and tris(trimethylsilyl) borate),[44,45] which improve the cycling stability of LLOs to various extents. Furthermore, our previous work demonstrated that boracic electrolyte additives, such as trimethyl borate (TMB) and triethyl borate (TEB), show great capability to enhance the cycling stability of LLOs.[33,35] Although tripropyl borate (TPB), whose structure is similar to that of TMB and TEB, has been demonstrated to improve the capacity retention and rate capability of a MCMB/$Li_{1.1}[Mn_{1/3}Ni_{1/3}Co_{1/3}]_{0.9}O_2$ full cell as

Engineering Research Center of MTEES (Ministry of Education), Research Center of BMET (Guangdong Province), Key Lab. of ETESPG (GHEI), Innovative Platform for ITBMD (Guangzhou Municipality), School of Chemistry and Environment, South China Normal University, Guangzhou 510006, China. E-mail: xingld@scnu.edu.cn; liwsh@scnu.edu.cn

† Electronic supplementary information (ESI) available. See DOI: 10.1039/c8ra03852j

an anion receptor additive,[46] no prior study has been performed to investigate its film-forming capability and influence on the cycling stability of high voltage LLOs.

In this work, the film-forming mechanism of TPB and its influence on the long-term cycling performance of a LLO were investigated systematically. Electrochemical and physical characterization demonstrated that the structural destruction of the LLO within and after 120 cycles is mainly caused by the dissolution of Ni and Mn ions, respectively. Addition of a small amount of TPB additive effectively suppresses the electrolyte oxidation and structural destruction of the LLO *via* generating a protective compact SEI film on the LLO surface, resulting in a greatly improved cycling stability of the high voltage LLO. Importantly, the capacity retention of the LLO achieved by the application of TPB is higher than most of the reported literature values, as shown in Table S1 (see ESI†).

2. Experimental

2.1 Electrode and electrolyte preparation

In this work, LLO ($Li_{1.2}Mn_{0.54}Ni_{0.13}Co_{0.13}O_2$) powders were synthesized by a sol–gel method, as in our previous works.[35,47] For the preparation of the LLO cathode and assembly of Li/LLO refer to our previous work.[35]

The standard (STD) (Tinci, China) electrolyte consists of 1.0 M $LiPF_6$ in a mixed solvent of ethylene carbonate (EC)/ethyl methyl carbonate (EMC)/diethyl carbonate (DEC) (3/5/2 by weight). Various amounts of TPB (1, 2, 3, and 4 wt%) (Aladdin, China) were added into the STD electrolyte to obtain an additive-containing electrolyte. For the preparation of all the electrolytes, refer to our previous work.[35]

2.2 Electrochemical measurement and physical characterization

The charging/discharging tests and electrochemical impedance measurement (EIS) of the Li/LLO coin cells were performed as in our previous work.[35] The V-type cells were charged at 0.1C with a cut-off voltage of 4.8 V and then maintained at 4.8 V for 3 days.

To understand the capacity fading mechanism of the LLO electrodes upon short- and long-term cycling, nuclear magnetic resonance (NMR, Agilent VNMRS-600 spectrometer, USA), X-ray photoelectron spectroscopy (XPS, ESCALAB 250Xi, USA), inductively coupled plasma atomic emission spectrometry (ICP AES, IRIS Intrepid II XSP, USA), scanning electron microscopy (SEM, JSM-6510, Japan) and transmission electron microscopy (TEM, JEM-2100, Japan) were performed. ^{19}F NMR spectra were acquired to clarify the role of TPB in suppressing electrolyte oxidation and decomposition after storage at 4.8 V (V-type cell) with acetonitrile-d3. ^{19}F NMR resonances were referenced to $LiPF_6$ at −74 and −76 ppm.[48] DMC solvent was used to wash off the residual electrolyte on the cycled electrodes before subsequent physical characterizations.

3. Results and discussion

Fig. 1 presents the cycling stability, coulombic efficiency, initial charge/discharge profiles and corresponding dQ/dV curves of

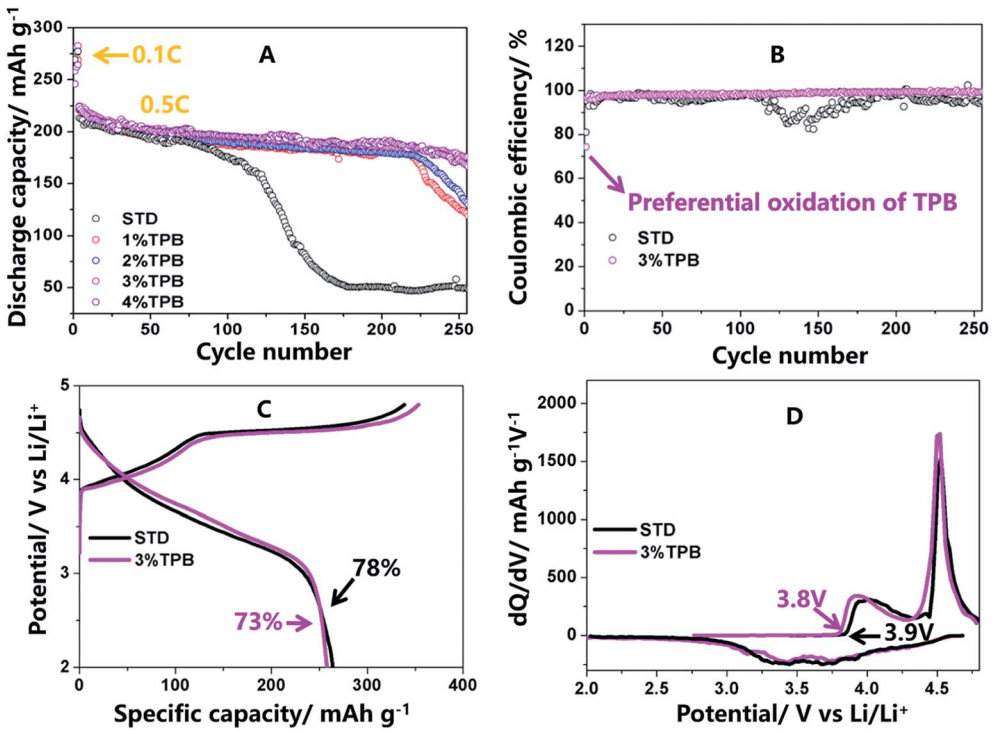

Fig. 1 (A) Cycling stability at 0.5C (1C = 250 mA g^{-1}) after an initial three cycles at 0.1C; (B) the corresponding coulombic efficiency; (C) the initial charge/discharge profiles at 0.1C rate; (D) the dQ/dV profiles of the LLO in the first charge process.

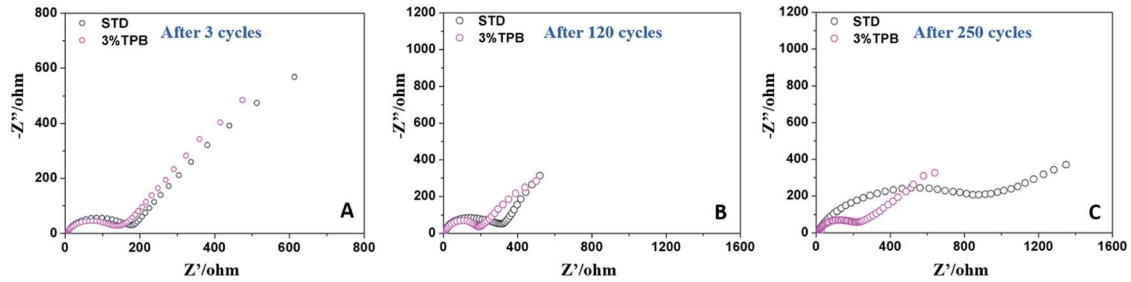

Fig. 2 Electrochemical impedance spectra of the LLO after cycling in STD and 3% TPB-containing electrolytes after 3 cycles (A), 120 cycles (B) and 250 cycles (C).

the LLO/Li cells in electrolytes with and without TPB. It can be seen from Fig. 1A that the discharge capacity of LLO cycled in STD electrolyte declines slowly within 120 cycles at 0.5C, which is mainly caused by the continuous decomposition of the STD electrolyte at high voltage and the layered-to-spinel phase transformation of the LLO.[32,33,36,49] However, after 120 cycles, the capacity of LLO with the STD electrolyte drops dramatically, resulting in a capacity retention of 21% after 250 cycles, which could be ascribed to the further structural damage of the generated spinel phase.[32,33,36] Interestingly, the addition of the TPB additive greatly suppressed the capacity fading of the LLO/Li cell. Specifically, the capacity retention of LLO/Li cells with 1%, 2%, 3% and 4% TPB-containing electrolytes was 55%, 59%, 78% and 76% after 250 cycles. The inferior cycling stability of the LLO/Li cells with 1% and 2% TPB-containing electrolytes can be explained by the inadequate amount of TPB additive. The capacity retentions of the LLO/Li cells with 3% and 4% TPB additive are similar and obviously higher than that of the 1% and 2% cells, indicating that 3% TPB additive is sufficient for LLO/Li cells. Next, the mechanism *via* which the 3% TPB additive improved the cycling stability of the LLO/Li cell was systematically investigated in this work.

As shown in Fig. 1B and C, the initial coulombic efficiency of the LLO/Li cell cycling in 3% TPB-containing electrolyte is 5% lower than that cycling in the STD electrolyte, suggesting the co-decomposition reaction of the TPB additive.[32,33,35,36,50] Importantly, in comparison with the STD electrolyte, the subsequent coulombic efficiency of the LLO/Li cell with 3% TPB-containing electrolyte becomes higher and steadier, confirming the great capability of the TPB additive to improve the interfacial stability of high voltage electrodes/electrolytes. The initial charging/discharging profiles (Fig. 1C) and the corresponding dQ/dV curves (Fig. 1D) of the LLO/Li cells consist of two stages: the stage below 4.5 V is ascribed to the oxidation of Ni^{2+} and Co^{3+}, and the other long voltage plateau at around 4.5 V corresponds to the activation of Li_2MnO_3.[41] The slightly lower onset oxidation potential of LLO/Li with the TPB additive can be observed from Fig. 1D, suggesting the preferential oxidation of the TPB additive.

Fig. 2 presents the impedance spectra of LLO/Li cells after 3, 120 and 250 cycles, which consist of a depressed semicircle at high frequency and a sloped line at low frequency. The semicircle reflects the electrode/electrolyte interfacial impedance, while the sloped line represents the diffusion of lithium ions in the electrode.[51] After 3 cycles, the difference between the interfacial resistances of the LLO/Li cells with and without the additive is negligible. However, the interfacial resistance of the LLO/Li cell in STD electrolyte keeps growing during cycling. It can be noted that the increase of the interfacial resistance of the LLO/Li with STD electrolyte is slow and fast before and after 120 cycles, which is consistent with the change of capacity fading of LLO/Li with STD electrolyte shown in Fig. 1A. The slow increase of resistance before 120 cycles can be ascribed to the rise of electrode polarization caused by electrolyte decomposition, while the one after 120 cycles is due to the breakdown of the electronic conduction network (shedding of the LLO particulates).[36] In contrast, the interfacial resistance of the LLO/Li cell with TPB stays almost constant in the subsequent cycles, indicating that the TPB additive not only suppresses the electrolyte oxidation and decomposition, but also hinders the structural destruction of the LLO.

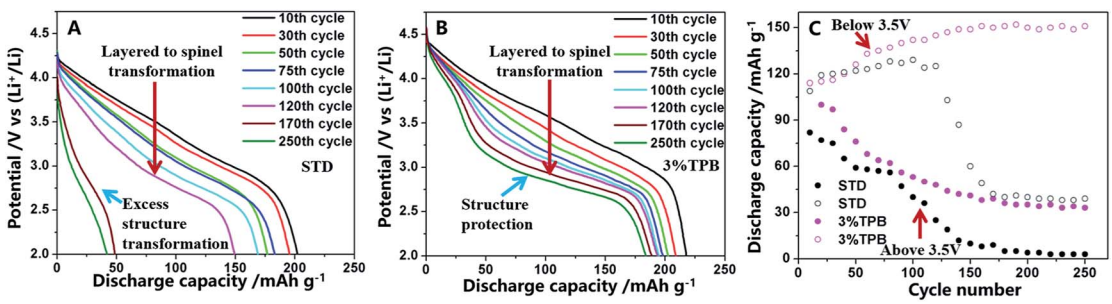

Fig. 3 Selected discharge curves of the LLO cycled in STD (A) and 3% TPB-containing (B) electrolytes at 0.5C rate and the discharge capacity (C) of the selected cycles above and below 3.5 V in both electrolytes.

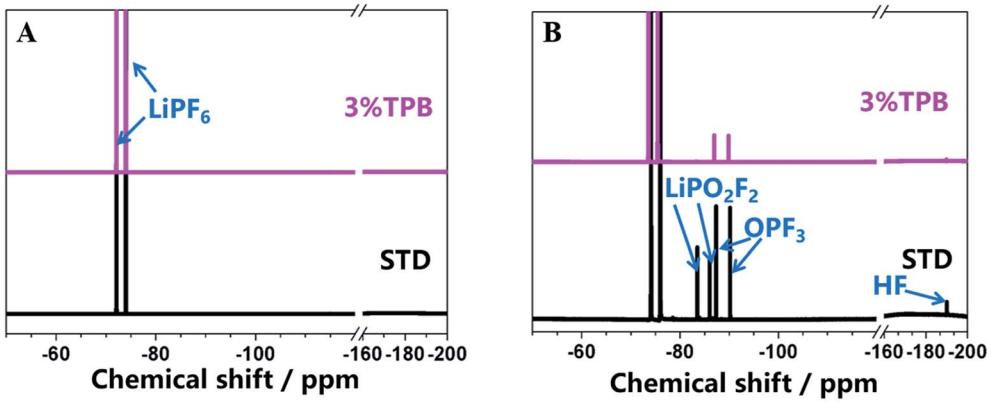

Fig. 4 ^{19}F NMR spectra of the STD and 3% TPB-containing electrolyte before (A) and after (B) the V-cell test.

Selected discharge curves and the intersected discharge capacity above and below 3.5 V are presented in Fig. 3. As shown in Fig. 3A and B, in contrast to the cell with the STD electrolyte, whose voltage platform almost disappeared at the end of the 250th cycle, the discharge platform of the LLO/Li cell with 3% TPB-containing electrolyte drops to around 3.0 V and is maintained well in the subsequent cycles. The voltage decay to 3.0 V has been proved to be ascribed to the phase transformation from a layered to a spinel-like structure of LLO.[36,52] Therefore, the change of the discharge voltage platform reveals that 3% TPB greatly improves the stability of the generated spinel phase structure of LLO, resulting in high capacity retention as shown in Fig. 1A. According to the reported literature,[49,52] the discharge capacity of a LLO/Li cell includes capacity above and below 3.5 V, which is ascribed to the lithium deintercalation from the layered and spinel structure of the LLO, respectively. As shown in Fig. 3C, the discharge capacity of the LLO above 3.5 V decreases monotonously during cycling, while the capacity below 3.5 V shows the reverse effect, confirming the phase transformation of the LLO during cycling.[49] Surprisingly, the capacity of the LLO/Li with the STD electrolyte, both above and below 3.5 V, decreases dramatically after 120 cycles, which clearly indicates the structural destruction of the LLO, including the remaining layered and generated spinel structure. This observation is in good agreement with the change of interfacial reaction resistance. However, after 170 cycles, the capacity of the LLO/Li with the TPB additive above and below 3.5 V stabilizes at around 32 and 150 mA h g^{-1}, respectively, further confirming the great capability of the TPB additive to enhance the structural stability of the LLO, especially the generated spinel structure. The coexistence of two phase structures of LLO with the TPB additive reveals that the layered-to-spinel phase transformation reaction could be inhibited by stabilizing the generated spinel phase.

In our previous work, we have theoretically and experimentally demonstrated that the oxidation reaction of the carbonate-based electrolyte generates HF, which would accelerate the dissolution of transition metal ions from the cathode.[36,53–55] Therefore, the ability of TPB to improve the cycling stability of LLO/Li cells may also rely on its suppression of electrolyte oxidation and the generation of HF. Fig. 4 presents the ^{19}F NMR spectra of the STD and 3% TPB-containing electrolytes in a V-type cell after maintaining a constant voltage of 4.8 V for 3 days. The peaks at −74 and −76 ppm in the ^{19}F NMR spectra are the characteristic peaks of $LiPF_6$, which both appear in the STD and 3% TPB-containing electrolytes. The appearance of $LiPO_2F_2$ (−83 and −86 ppm), OPF_3 (−87 and −90 ppm) and HF (190 ppm)[56] confirms the oxidation of the electrolyte after storage at high voltage. It can be easily seen from Fig. 4 that the peaks of $LiPO_2F_2$, OPF_3 and HF in the 3% TPB-containing electrolyte after storage are obviously weaker than those of the STD electrolyte, confirming that the preferential oxidation of TPB suppresses the oxidation of the STD electrolyte and the subsequent generation of HF, which may result in less transition metal dissolution. Indeed, as shown in Fig. 5, the detected content of Mn, Ni and Co on the lithium plate cycled with TPB is obviously lower in comparison to that of the STD electrolyte. It is important to mention that after 120 cycles, for the lithium plate with the STD electrolyte, the detected content of Ni is higher than that of Mn, while after 250 cycles, the content of Mn

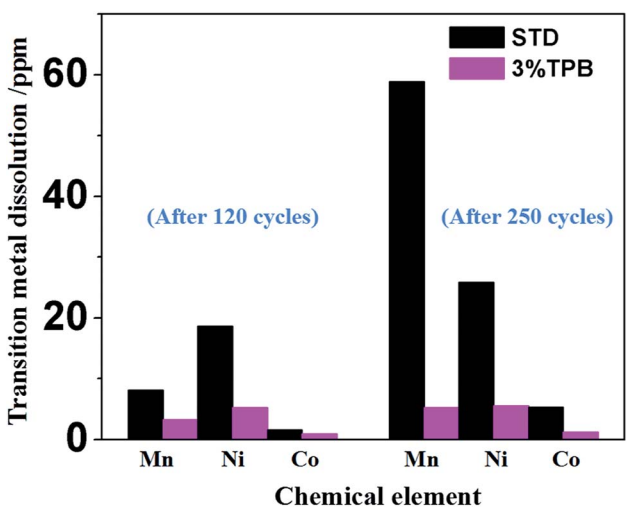

Fig. 5 Contents of the deposited transition metals on the lithium electrode after 120 cycles and 250 cycles in STD and 3% TPB-containing electrolytes.

becomes obviously higher than that of Ni. In combination with the cycling stability of the LLO/Li cell with STD electrolyte shown in Fig. 1A, it can be concluded that the structural destruction of the LLO cell during short and long-term cycling is mainly caused by the dissolution of Ni and Mn, respectively.

The interfacial composition of the cycled LLO electrodes was analyzed by XPS, with the obtained results presented in Fig. 6. The C 1s, O 1s, F 1s and P 2p XPS spectra of fresh LLO and the LLO after 250 cycles in STD and 3% TPB-containing electrolytes are given in Fig. 6A. In the C1s spectra, the peaks at 290.3 and 285.7 eV correspond to the PVDF binder, while the peak at 284.8 eV is ascribed to acetylene black. The peak intensity of PVDF and acetylene black after cycling with the STD electrolyte is weaker than that after cycling with the 3% TPB-containing electrolyte, indicating that the deposition of the electrolyte decomposition products in the former case is thicker than that in the latter. The C=O (289 eV) and C–O (286 eV) peaks that correspond to electrolyte decomposition products such as $ROCO_2Li$, ROLi and Li_2CO_3 (ref. 57) after cycling in the STD electrolyte are stronger than those for the 3% TPB-containing electrolyte, further confirming the capability of 3% TPB to suppress electrolyte oxidation. In the O 1s spectra, the peak at 529.9 eV is ascribed to the metallic oxide (Me-O), while the C=O (531.7 eV) and C–O (533.4 eV) peaks are assigned to the polycarbonates generated from electrolyte decomposition.[58–63] The stronger Me-O and weaker C=O and C–O peaks in the O 1s

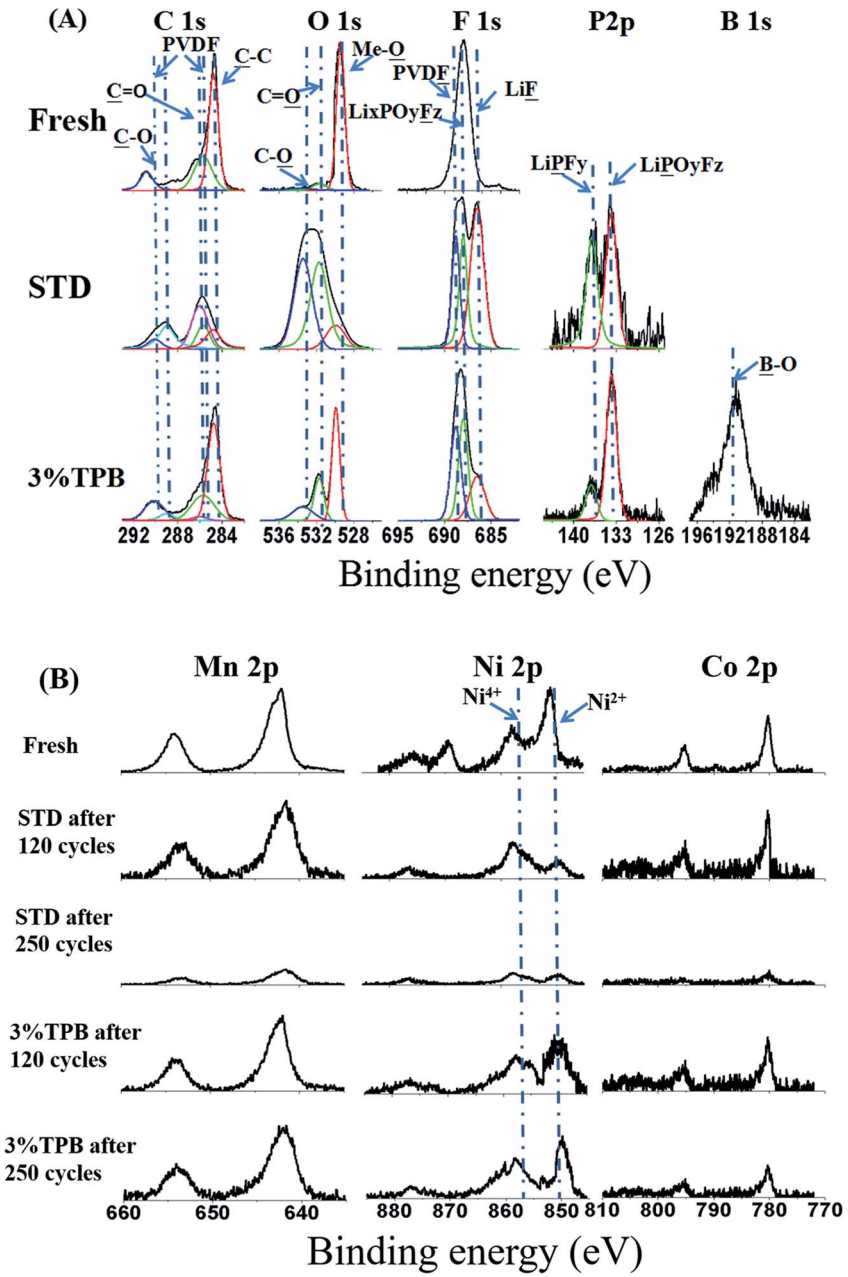

Fig. 6 The C 1s, O 1s, F 1s and P 2p (A) and Mn 2p, Ni 2p and Co 2p (B) XPS spectra of fresh LLO electrodes and the LLO electrodes cycled in STD and 3% TPB-containing electrolytes.

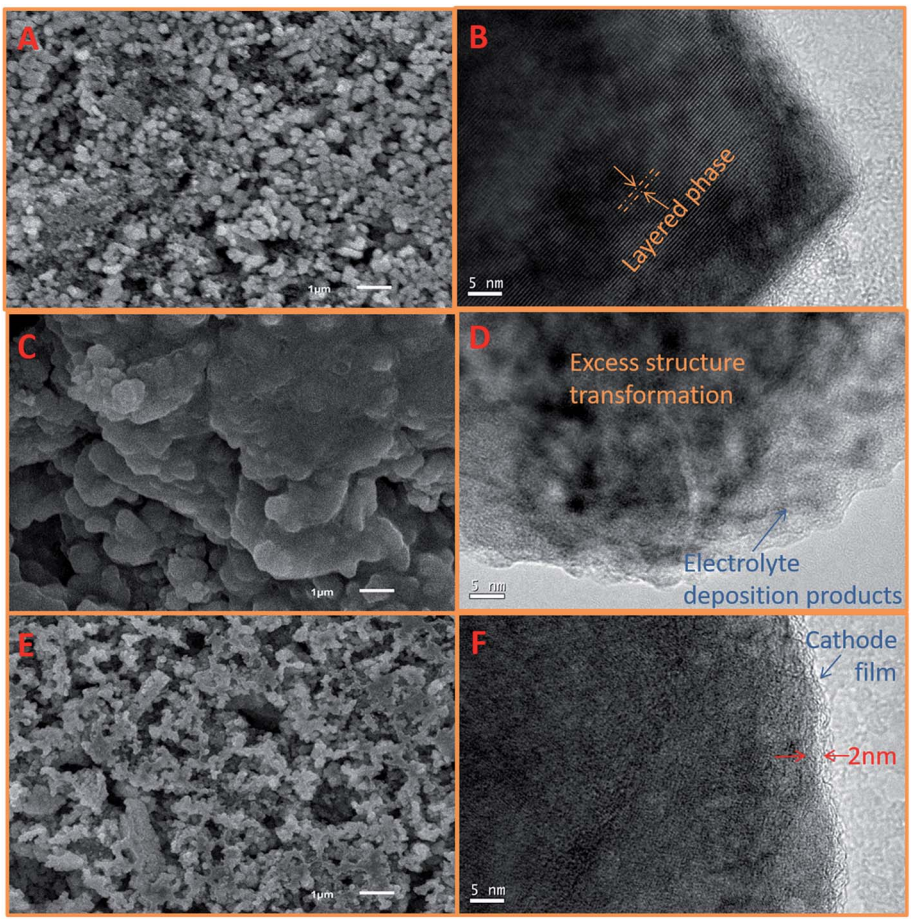

Fig. 7 SEM and TEM images of fresh LLO (A and B) and LLO in STD (C and D) and 3% TPB-containing (E and F) electrolytes after 250 cycles at 0.5C rate.

spectrum of the 3% TPB electrolyte system also confirms the thinner layer of decomposition products after cycling. Similarly, in the F 1s and P 2p spectra, the LiF and $Li_xPO_yF_z$ peaks, which reflect the co-decomposition of $LiPF_6$, are weaker in STD electrolyte than in 3% TPB-containing electrolyte.

Fig. 6B presents the Mn 2p, Ni 2p and Co 2p XPS spectra of a fresh LLO electrode and the LLO electrodes after 120 and 250 cycles. In the Ni 2p spectra, there are peaks of Ni^{4+} and Ni^{2+} at 856 eV and 850 eV, respectively.[64] It is obvious that the peak of Ni^{2+} for the LLO with the STD electrolyte becomes weaker than that of Ni^{4+} after 120 cycles, and both peaks almost disappear after 250 cycles. Gu *et al.* proposed that Ni ions would preferentially segregate on the surface facets during cycling,[65] and this segregated Ni may be easily dissolved, leading to fast voltage fading of the LLO and the transformation of the structure from layer to spinel.[66] This in good agreement with our observation of more severe Ni dissolution after 120 cycles in STD electrolyte (see Fig. 5). In contrast, the change of Mn 2p and Co 2p of the LLO in STD electrolyte after 120 cycles is negligible. After 250 cycles, the peaks of Mn 2p, Ni 2p and Co 2p almost disappear, which can be ascribed to the thick covering of electrolyte decomposition products and the dissolution of metal ions. However, the peak intensities in the Mn 2p, Ni 2p and Co 2p spectra of the LLO after cycling in 3% TPB-containing electrolyte remain similar to those of the fresh one, confirming the great capability of TPB to suppress the structural damage of the LLO and electrolyte decomposition.

Fig. 7 presents the SEM and TEM images of the fresh and cycled LLO in STD and 3% TPB-containing electrolyte. A smooth and clean surface (Fig. 7A) and obvious layered structure (Fig. 7B) can be observed on the fresh LLO particles.[41] The detailed lattice fringe presents the typical crystal (001) plane of Li_2MnO_3 and (003) plane of $LiMn_{1/3}Ni_{1/3}Co_{1/3}O_2$.[35] However, after cycling in STD electrolyte, as shown in Fig. 7C and D, the LLO surface is apparently covered by a thick and irregular polymer film resulting from the continuous decomposition of the STD electrolyte at high voltage.[67] Moreover, the LLO particles lose their crystal feature, indicating their severe structural damage after 250 cycles. In contrast, the surface morphology of the LLO cycled in 3% TPB-containing electrolyte compares well with the fresh one, see Fig. 7A and E, except that there is a uniform thin SEI film covering the LLO surface after 250 cycles with the TPB additive (see Fig. 7F).

4. Conclusion

It has been demonstrated in this work that the capacity fading of LLO/Li cells during short-term cycling is mainly caused by

electrolyte decomposition and layered-to-spinel phase transformation, while that during long-term cycling is triggered by structural destruction of the generated spinel phase. The ICP results reveal that Ni dissolution is more severe than Mn and Co dissolution within 120 cycles; however, Mn dissolution becomes even worse in the subsequent cycles. Tripropyl borate (TPB) as an electrolyte film-forming additive shows higher oxidation activity than STD electrolyte, and generates a condensed protective SEI film on the LLO surface during the initial charging process, resulting in a significantly improved cycling stability of high voltage LLO/Li cells. This TPB-derived SEI film suppresses the continuous oxidation of the electrolyte, and therefore hinders the generation of harmful decomposition products, especially HF, which plays an important role in restraining the transition metal dissolution and structural destruction of the LLO during cycling.

Conflicts of interest

There are no conflicts to declare.

Acknowledgements

This work was supported by the National Natural Science Foundation of China (21573080), Guangdong Program for Support of Top-notch Young Professionals (2015TQ01N870) and Distinguished Young Scholars (2017B030306013), and the Science and Technology Planning Project of Guangdong Province (Grant No. 2017B090901020).

References

1 H. B. Rong, M. Q. Xu, L. D. Xing and W. S. Li, *J. Power Sources*, 2014, **261**, 148.
2 M. M. Thackeray, C. Wolverton and E. D. Isaacs, *Energy Environ. Sci.*, 2012, **5**, 7854.
3 J. M. Tarascon and M. Armand, *Nature*, 2001, **414**, 359.
4 M. Armand and J. M. Tarascon, *Nature*, 2008, **451**, 652.
5 J. Tollefson, *Nature*, 2008, **456**, 436.
6 J. B. Goodenough and Y. Kim, *Chem. Mater.*, 2010, **22**, 587.
7 L. W. Su, Y. Jing and Z. Zhou, *Nanoscale*, 2011, **3**, 3967.
8 J. Zhao, W. H. Li, H. Z. Xu, L. S. Sun, C. Q. Li and F. Q. Liu, *RSC Adv.*, 2016, **6**, 70972.
9 S. Byun, J. Park, W. A. Appiah, M. H. Ryou and Y. M. Lee, *RSC Adv.*, 2017, **7**, 10915.
10 S. Y. Zuo, Z. G. Wu, S. K. Li, D. Yan, Y. H. Liu, F. Y. Wang, R. F. Zhuo, B. S. Geng, J. Wang and P. X. Yan, *RSC Adv.*, 2017, **7**, 18054.
11 K. Kang, Y. S. Meng, J. Breger, C. P. Grey and G. Ceder, *Science*, 2006, **311**, 977.
12 A. R. Armstrong, M. Holzapfel, P. Novak, C. S. Hohnson, S. H. Kang, M. M. Thackeray and P. G. Bruce, *J. Am. Chem. Soc.*, 2006, **128**, 8694.
13 Z. H. Lu, D. D. MacNeil and J. R. Dahn, *Electrochem. Solid-State Lett.*, 2001, **4**, A191.
14 A. D. Robertson and P. G. Bruce, *Chem. Mater.*, 2003, **15**, 1984.
15 Y. W. Denis, K. Yanagida, Y. Kato and H. Nakamura, *J. Electrochem. Soc.*, 2009, **156**, A417.
16 S. H. Yu, T. Yoon, J. Mun, S. Park, Y. S. Kang, J. H. Park, S. M. Oh and Y. E. Sung, *J. Mater. Chem. A*, 2013, **1**, 2833.
17 Y. S. Kang, T. Yoon, S. S. Lee, J. Mun, M. S. Park, J. H. Park, S. G. Doo, L. Y. Song and S. M. Oh, *Electrochem. Commun.*, 2013, **27**, 26.
18 F. Rosciano, J. F. Colin, F. L. Mantia, N. Tran and P. Novak, *Electrochem. Solid-State Lett.*, 2009, **12**, A140.
19 B. Xu, C. R. Fell, M. Chi and Y. S. Meng, *Energy Environ. Sci.*, 2011, **4**, 2223.
20 H. J. Yu, H. J. Kim, Y. R. Wang, P. He, D. Asakura, Y. Nakamura and H. S. Zhou, *Phys. Chem. Chem. Phys.*, 2012, **14**, 6584.
21 A. Boulineau, L. Simonin, J. F. Colin, C. Bourbon and S. Patoux, *Nano Lett.*, 2013, **13**, 3857.
22 J. M. Zheng, M. Gu, J. Xiao, P. J. Zuo, C. M. Wang and J. G. Zhang, *Nano Lett.*, 2013, **13**, 3824.
23 G. S. Zou, X. K. Yang, X. Y. Wang, L. Ge, H. B. Shu, Y. S. Bai, C. Wu, H. P. Guo, L. Hu, X. Yi, *et al.*, *J. Solid State Electrochem.*, 2014, **18**, 1789.
24 Z. Y. Wang, E. Z. Liu, L. C. Guo, C. S. Shi, C. N. He, J. J. Li and N. Q. Zhao, *Surf. Coat. Technol.*, 2013, **235**, 570.
25 G. R. Li, X. Feng, Y. Ding, S. H. Ye and X. P. Gao, *Electrochim. Acta*, 2012, **78**, 308.
26 X. Y. Liu, J. L. Liu, T. Huang and A. S. Yu, *Electrochim. Acta*, 2013, **109**, 52.
27 D. H. Cho, H. Yashiro, Y. K. Sun and S. T. Myung, *J. Electrochem. Soc.*, 2014, **161**, A142.
28 R. P. Qing, J. L. Shi, D. D. Xiao, X. D. Zhang, Y. X. Yin, Y. B. Zhai, L. Gu and Y. G. Guo, *Adv. Energy Mater.*, 2015, **5**, 1501914.
29 Z. Zheng, X. D. Guo, Y. J. Zhong, W. B. Hua, C. H. Shen, S. L. Chou and X. S. Yang, *Electrochim. Acta*, 2016, **188**, 336.
30 R. Yu, G. Wang, M. Liu, X. Zhang, X. Wang, H. Shu, X. Yang and W. Huang, *J. Power Sources*, 2016, **335**, 65.
31 R. Yu, X. Wang, Y. Fu, L. Wang, S. Cai, M. Liu, B. Lu, G. Wang, D. Wang, Q. Ren and X. Yang, *J. Mater. Chem. A*, 2016, **4**, 4941.
32 J. Li, L. Xing, R. Zhang, M. Chen, Z. Wang, M. Xu and W. Li, *J. Power Sources*, 2015, **285**, 360.
33 J. Li, L. Xing, L. P. Zhang, L. Yu, W. Z. Fan, M. Q. Xu and W. S. Li, *J. Power Sources*, 2016, **324**, 17.
34 J. G. Han, S. J. Lee, J. Lee, J. S. Kim, K. T. Lee and N. S. Choi, *ACS Appl. Mater. Interfaces*, 2015, **7**, 8319.
35 J. Li, L. Zhang, L. Yu, W. Fan, Z. Wang, X. Yang, Y. Lin, L. Xing, M. Xu and W. Li, *J. Phys. Chem. C*, 2017, **120**, 26899.
36 J. Li, L. Xing, J. Chen, H. Zhou, M. Xu and W. Li, *J. Electrochem. Soc.*, 2016, **163**, A2258.
37 A. M. Haregewoin, A. S. Wotango and B. J. Hwang, *Energy Environ. Sci.*, 2016, **9**, 1955.
38 L. Wang, Y. Ma, Q. Lin, Z. Zhou, X. Cheng, P. Zuo, C. Du, Y. Gao and G. Yin, *J. Power Sources*, 2016, **361**, 227.
39 P. Hong, M. Xu, X. Zheng, Y. Zhu, Y. Liao, L. Xing, Q. Huang, H. Wan, Y. Yang and W. Li, *J. Power Sources*, 2016, **329**, 216.
40 Z. D. Li, Y. C. Zhang, H. F. Xiang, X. H. Ma, Q. F. Yuan, Q. S. Wang and C. H. Chen, *J. Power Sources*, 2013, **240**, 471.

41 W. Tu, P. Xia, X. Zheng, C. Ye, M. Xu and W. Li, *J. Power Sources*, 2017, **341**, 348.
42 Z. Zhou, Y. Ma, L. Wang, P. Zuo, X. Cheng, C. Du, G. Yin and Y. Gao, *Electrochim. Acta*, 2016, **216**, 44.
43 J. Pires, A. Castets, L. Timperman, J. Santos-Peña, E. Dumont, S. Levasseur, C. Tessier, R. Dedryvère and M. Anouti, *J. Power Sources*, 2015, **296**, 413.
44 S. H. Lim, W. Cho, Y. Kim and T. Yim, *J. Power Sources*, 2016, **336**, 465.
45 A. Birrozzi, N. Laszczynski, M. Hekmatfar, J. Zamory, G. Giffin and S. Passerini, *J. Power Sources*, 2016, **325**, 525.
46 Z. H. Chen, J. Liu and K. Amine, *Electrochim. Acta*, 2008, **53**, 3267.
47 M. Chen, X. Xiang, D. Chen, Y. Liao, Q. Huang and W. Li, *J. Power Sources*, 2015, **279**, 197.
48 M. H. Liu, F. Dai, Z. Ma, M. Ruthkosky and L. Yang, *J. Power Sources*, 2014, **268**, 37.
49 B. H. Song, Z. W. Liu, M. O. Lai and L. Lu, *Phys. Chem. Chem. Phys.*, 2012, **14**, 12875.
50 X. R. Yang, J. H. Li, L. D. Xing, Y. H. Liao, M. Q. Xu, Q. M. Huang and W. S. Li, *Electrochim. Acta*, 2017, **227**, 24.
51 J. Zhang, J. Wang, J. Yang and Y. N. Li, *Electrochim. Acta*, 2014, **117**, 99.
52 J. M. Zheng, M. Gu, A. Genc, J. Xiao, P. H. Xu, X. L. Chen, Z. H. Zhu, W. B. Zhao, L. Pullan, C. M. Wang, *et al.*, *Nano Lett.*, 2014, **14**, 2628.
53 Y. M. Zhu, X. Y. Luo, M. Q. Xu, L. P. Zhang, L. Yu, W. Z. Fan and W. S. Li, *J. Power Sources*, 2016, **317**, 65.
54 L. Xing, O. Borodin, G. Smith and W. Li, *J. Phys. Chem. A*, 2011, **115**, 13896.
55 Y. T. Wang, L. D. Xing, W. S. Li and D. Bedrov, *J. Phys. Chem. Lett.*, 2013, **4**, 3992.
56 M. Xu, L. Hao, Y. Liu, W. Li, L. Xing and B. Li, *J. Phys. Chem. C*, 2011, **115**, 6085.
57 X. X. Zuo, C. J. Fan, J. S. Liu, X. Xiao, J. H. Wu and J. M. Nan, *J. Power Sources*, 2013, **229**, 308.
58 B. Li, Y. Q. Wang, H. B. Lin, J. S. Liu, L. D. Xing, M. Q. Xu and W. S. Li, *Electrochim. Acta*, 2014, **14**, 263.
59 P. Verma, P. Maire and P. Novák, *Electrochim. Acta*, 2010, **55**, 6332.
60 M. Xu, A. Xiao, W. Li and B. L. Lucht, *J. Electrochem. Soc.*, 2010, **157**, A115.
61 D. Aurbach, I. Weissman, A. Schechter and H. Cohen, *Langmuir*, 1996, **12**, 3991.
62 W. Li, A. Xiao, B. L. Lucht, M. C. Smart and B. V. Ratnakumar, *J. Electrochem. Soc.*, 2008, **155**, A648.
63 Y. Yang, T. Markmaitree and B. L. Lucht, *J. Power Sources*, 2011, **196**, 2251.
64 X. Wei, S. Zhang, Z. Du, P. Yang, J. Wang and Y. Ren, *Electrochim. Acta*, 2013, **107**, 549.
65 M. Gu, I. Belharouak, A. Genc, D. Wang, Z. Wang, K. Amine, F. Gao, G. Zhou, S. Thevuthasan, D. R. Baer, *et al.*, *Nano Lett.*, 2012, **12**, 5186.
66 J. Zheng, S. Myeong, W. Cho, P. Yan, J. Xiao, C. Wang, J. Cho and J. Zhang, *Adv. Energy Mater.*, 2017, **7**, 1601284.
67 W. N. Huang, L. D. Xing, Y. T. Wang, M. Q. Xu, W. S. Li, F. C. Xie and S. G. Xia, *J. Power Sources*, 2014, **267**, 560.